Nanoscale

Accepted Manuscript

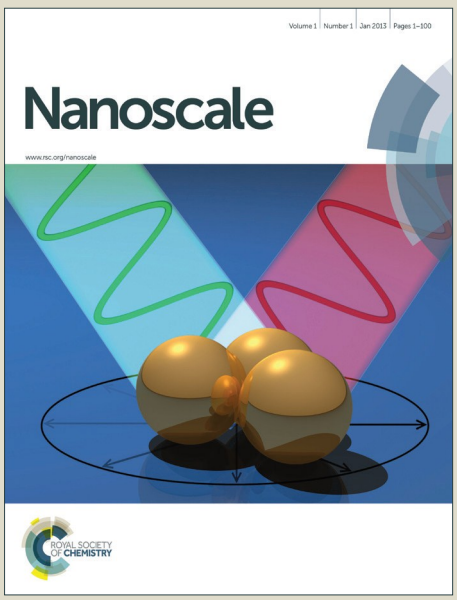

ROYAL SOCIETY OF CHEMISTRY

www.rsc.org/nanoscale

T-type Method for Characterization of the Thermoelectric Performance of an Individual Free-Standing Single Crystal Bi_2S_3 Nanowire

Weigang Ma, ‡,[a] Tingting Miao, ‡,[a,b] Xing Zhang,*,[a] Koji Takahashi,[c] Tatsuya Ikuta,[c] Boping Zhang,[d] Zhenhua Ge[d]

[a]*Key Laboratory for Thermal Science and Power Engineering of Ministry of Education, Department of Engineering Mechanics, Tsinghua University, Beijing 100084, China. Email: x-zhang@tsinghua.edu*

[b]*Beijing Key Laboratory of Process Fluid Filtration and Separation, College of Mechanical and Transportation Engineering, China University of Petroleum, Beijing 102249, China*

[c]*Department of Aeronautics and Astronautics, Graduate school of Engineering, Kyushu University, Fukuoka 819-0395, Japan*

[d]*Beijing Key Lab of New Energy Materials and Technology, School of Materials Science and Engineering, University of Science and Technology Beijing, Beijing, 100083, China*

‡*These authors contributed equally to this work.*

A comprehensive method to evaluate the thermoelectric performance of one-dimensional nanostructures, called T-type method, has been first developed. The thermoelectric properties, including Seebeck coefficient, thermal conductivity and electrical conductivity, of an individual free-standing single crystal Bi_2S_3 nanowire have been first characterized by applying the T-type method. The determined figure of merit is far less than the reported values of nanostructured bulk Bi_2S_3 samples, and the mechanism is that the Seebeck coefficient is nearly zero in the temperature range of 300 - 420 K and changes its sign at 320 K.

Introduction

Solid-state and direct energy conversion between heat and electricity based on thermoelectric effects without moving parts is attractive for many applications in low grade waste heat recovery and micro-gravity environment.[1,2] The performance of thermoelectric materials is quantified by a figure of merit, $ZT=S^2\sigma T/\lambda$, where T is the absolute working temperature, S, σ, and λ represent the Seebeck coefficient, electrical conductivity and thermal conductivity, respectively. The challenge to achieve superior thermoelectric performance amounts to tailoring the physically interconnected parameters S, σ and λ.[3] Hence, the ZT~1 ceiling persisted until the 1990s.[3,4] In recent years, nanotechnology provides a chance to decouple the thermal and electrical transport by changing in the density of states and introducing some new scattering mechanisms, and consequently opens the opportunity to improve the performance and expand the applications of thermoelectrics,[3-8] i.e., nanowires,[5] superlattices,[6] nanocomposites,[7] and quantum dots.[8] Evaluation of thermoelectric performance of new developed nanomaterials has turned out to be one of the most important and challenging issues in

the development and fundamental understanding of the nanoscale thermoelectric materials.[9,10] From the definition of the figure of merit, the Seebeck coefficient S, electrical conductivity σ, and thermal conductivity λ should be determined comprehensively to obtain the figure of merit ZT of thermoelectric nanomaterials. One strategy is to repeatedly attach and detach the same sample to determine these three parameters in different measurement device. The sample would be inevitably damaged during the attaching and detaching processes and may consequently change the thermoelectric properties, since in nanoscale the property is very sensitive to the structure. The other strategy is to measure the three parameters on different samples of the same batch. The limitation is that there are significant individual differences in nanoscale materials. Hence, the optimum strategy is to comprehensively determine the thermoelectric performance of the same sample in the same measurement configuration. The most representative method is the suspended microfabricated device,[11,12] which has been widely applied in characterizing the thermoelectric properties of one-dimensional nanostructures.[5,13,14] However, Wingert *et al.*[15] found that in this method the background conductance is not negligible compared to that of the tested nanowire, especially when the thermal conductivity is small, due to near field thermal radiation energy exchange between the two membranes. In this paper, we first develop a T-type method to comprehensively characterize the thermoelectric performance of one-dimensional nanostructures.

Bismuth sulfide (Bi_2S_3) with direct bandgap of 1.3 eV[16] is a tellurium-free member of the family of compounds Pn_2X_3 (Pn = Sb, Bi and X= S, Se, Te), which are considered to be most promising for thermoelectric applications.[6,8] Bi-Te-based compounds[17] show the best room temperature thermoelectric properties. However, since tellurium is rare and toxic, the development of alternative materials is necessary and Bi_2S_3 has attracted increasing attention.

The best *ZT* values reported for the Bi_2S_3 system can reach 0.6.[18-20] The thermoelectric properties have been reported on bulk Bi_2S_3 with different types, including bulk single crystals,[21] single crystalline pellets,[22] whiskers,[23] ingots,[20,24] SPS-sintered polycrystalline bulk,[18,19,25-28] nanonetwork hot-pressed bulk,[29] nanowires-pressed film,[30] and nanorod self-assembled film.[31] However, the thermoelectric properties of an individual Bi_2S_3 nanowire has not been studied, which is important for fundamental study of the physical mechanism on the thermoelectric performance change from nanowire to nanostructured bulk, as from brick to building.

In this paper, the thermoelectric performance of an individual free-standing single crystal Bi_2S_3 nanowire has been characterized for the first time by applying our new developed T-type method. Fig. 1 illustrates the physical model of the T-type method and the scanning electron microscopy (SEM) image of the sample-attached T-type nanosensor including a Pt nanosensor, a tested Bi_2S_3 nanowire, and heat sink.

Experiment

An ac heating-dc detecting T-type mode is developed to detect the Seebeck coefficient. As shown in Fig. 1(a), the electrodes A, D are used to impose ac heating current, electrodes B, C are used to detect the ac current, and electrodes B, E are used to detect the corresponding dc thermoelectric voltage. The Pt nanofilm sensor serves simultaneously as a heater, a resistance thermometer and a lead wire. Since both ends of the nanofilm sensor and one end of the Bi_2S_3 nanowire are supported with the Pt frames which have much larger heat capacities compared to those of the nanofilm sensor and Bi_2S_3 nanowire, the temperatures of these spots can be maintained at the initial temperature, T_0, for the entire measurement. Feeding an electric current of the form $I_0\sin(\omega t)$ on the suspended nanofilm sensor, the temperature distribution of the

nanofilm, $T_f(x_f, t)$, contains static, $T_{f,static}(x_f, t)$, and harmonic, $T_{f,harmonic}(x_f, t)$, components due to Joule heating effect,

$$T_f\left(x_f, t\right) = T_{f,static}\left(x_f\right) + T_{f,harmonic}\left(x_f, t\right). \quad (1)$$

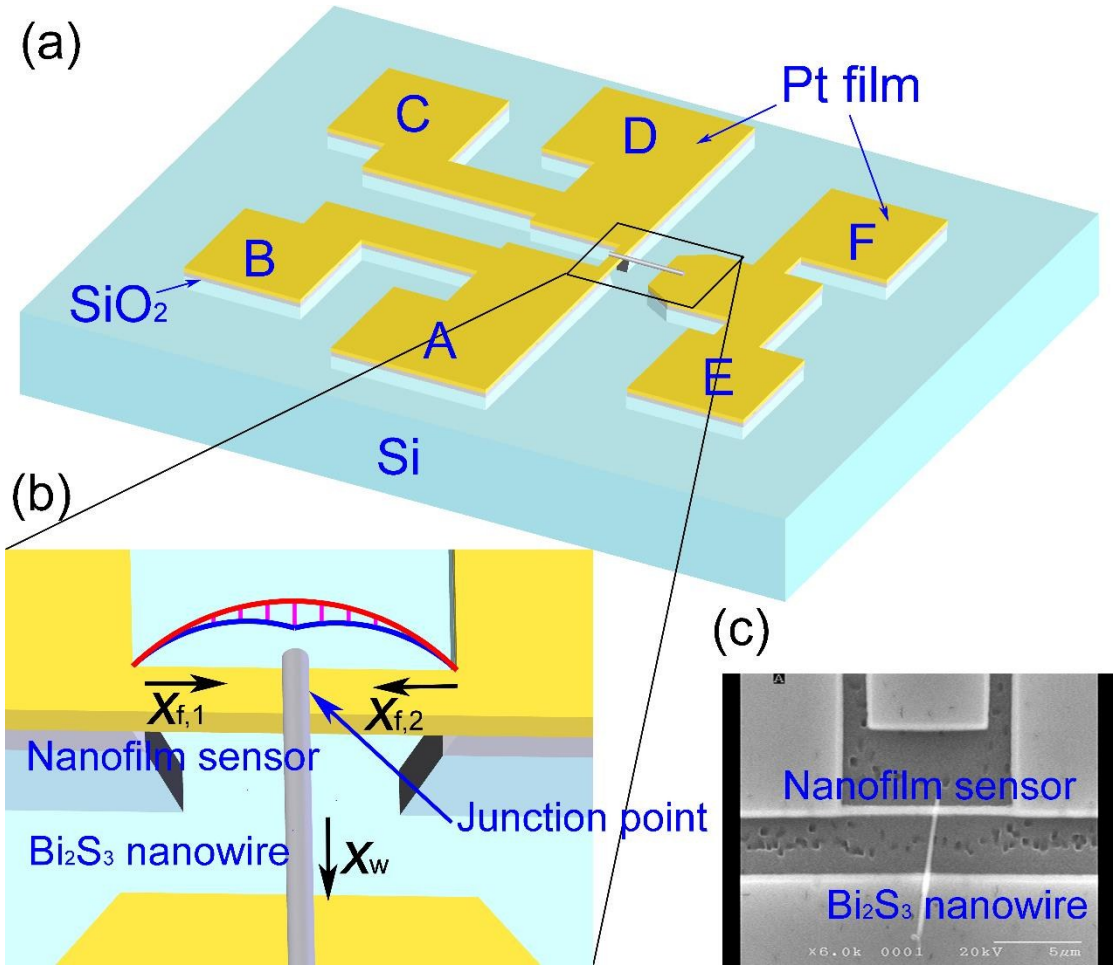

Fig. 1 Physical model of the T-type method.

Accordingly, the local temperature of the attached Bi_2S_3 nanowire at the junction point increases and serves as the "hot end", while the temperature of the nanowire at the heat sink side is maintained at the initial temperature T_0 and serves as the "cold end". Thus, the temperature difference between hot and cold ends of the Bi_2S_3 nanowire contains static and harmonic components,

$$\Delta T_w(t) = \Delta T_{w,static} + \Delta T_{w,harmonic}(t). \quad (2)$$

According to Seebeck effect, the static temperature difference will generate the corresponding dc thermoelectric voltage while the harmonic temperature difference generates ac thermoelectric voltage. Hence, detecting the dc electric voltage V_{dc} between two ends of the tested Bi_2S_3 nanowire from electrodes B and E, the Seebeck coefficient, S, can be extracted from,

$$S = -\frac{V_{dc}}{\Delta T_{w,static}}. \quad (3)$$

All the measurements are carried out at high vacuum (~10^{-4} Pa), the effects of heat losses from the heat conduction of rarefied gas and thermal radiation can be neglected.[32] Considering the Joule self-heating as internal heat source for the nanofilm sensor, the heat transfer process in the nanofilm sensor and tested Bi_2S_3 nanowire can be simplified into one-dimensional heat conduction along the longitudinal direction, imposed with continuity conditions of temperature and heat flow at the junction point. The static temperature difference across the nanowire, $\Delta T_{w,static}$, can be obtained,

$$\Delta T_{w,static} = 2\left(\Delta T_f - \frac{\left(l_{f,1}^3 + l_{f,2}^3\right)}{l_f^3}\Delta T_{f,calibration}\right) \quad (4)$$

where l_f is the overall length of the nanofilm sensor, $l_{f,1}$ and $l_{f,2}$ are the lengths of the left- and right-hand sides from the junction point, l_f=$l_{f,1}$+$l_{f,2}$. $\Delta T_{f,calibration}$ is the volumetric average temperature rise of the sensor determined from the resistance change during calibration when the applied heating current is $I_0\sin(\omega t)$ and the tested nanowire has not been attached. ΔT_f is the volumetric average temperature rise of the sensor during Seebeck coefficient determination when the applied heating current is the same as that applied in calibration, $I_0\sin(\omega t)$, and the tested nanowire has been attached on the sensor (see Supporting Information for derivation of eqn (4)).

The Seebeck coefficient of the Bi_2S_3 nanowire can be directly obtained. The highlight of the present ac heating-dc detecting T-type method is to establish the temperature difference between the hot and cold ends of the Bi_2S_3 nanowire by using ac current and to detect the corresponding dc thermoelectric voltage, which is effective to extract the weak thermoelectric voltage signal from the much larger heating electric voltage. The other merit of the present method on determining the Seebeck coefficient is that the required static temperature difference across the nanowire can be directly extracted from the resistance change determined volumetric average temperature rise of the nanofilm sensor before and after attachment of the tested nanowire for the same heating current, as illustrated in eqn (4). The length and diameter of the nanowire, and thickness as well as width of the nanofilm sensor need not be measured in Seebeck coefficient characterization, which is effective to reduce the measurement uncertainty. It is necessary to discuss why ac heating-dc detecting scheme instead of dc heating-dc detecting is applied in the Seebeck coefficient measurement. As illustrated in Fig. 1(a), electrodes A, D are used to impose heating current, and electrodes B, E are used to detect the corresponding thermoelectric voltage. If dc current is applied to heat the nanofilm sensor, as shown in Fig. 1(b), the dc ohmic voltage drop across the left branch of the nanofilm sensor from the junction point inevitably occurs. It is impossible to extract the weak dc thermoelectric voltage signal from the much larger ohmic voltage. By contrast, when ac heating current is applied, the dc ohmic voltage drop is zero and the weak dc thermoelectric voltage can be steadily determined.

A dc heating-dc detecting T-type mode is applied to detect the thermal conductivity of the Bi_2S_3 nanowire. Different from Seebeck coefficient measurement, the electrodes A, D are used to impose dc heating current instead of ac current, electrodes B, C are used to detect the corresponding dc voltage. The Pt nanofilm sensor serves as a heater and a resistance thermometer.

As illustrated in Fig. 1(b), as a dc current is passed through the Pt nanofilm sensor, the shape of the temperature distribution on the sensor changes from parabolic to dual-arch after the Bi_2S_3 nanowire is attached on the sensor, since the tested Bi_2S_3 nanowire serves as a heat conduction channel and part of the heat conducts from the sensor to the heat sink through the nanowire. Hence, the thermal conductivity of the nanowire, λ_w, can be extracted from comparing the average temperature change of the sensor without and with the attached nanowire for a given dc heating current,[32]

$$\lambda_w = \frac{\lambda_f A_f l_f l_w \left(q_v l_f^3 - 12\lambda_f l_f \Delta T_v\right)}{A_w l_{f,1} l_{f,2}\left[12\lambda_f l_f \Delta T_v - q_v\left(l_{f,1}^3 + l_{f,2}^3\right)\right]} \quad (5)$$

where λ_f and A_f are the thermal conductivity and cross section of the Pt nanofilm sensor. A_w and l_w are the cross section and length of suspended section of the Bi_2S_3 nanowire. ΔT_v is the average temperature rise of the sensor. $q_v=IV/(A_f l_f)$ is the volumetric heat generation rate of the electric current heating. I and V are the current and voltage applied.

The electrical conductivity of the nanowire can be determined by standard four-probe method in the T type frame as well. The electrodes A, E are used to impose the probing dc current and electrodes C, F are used to detect the corresponding voltage. The electrical resistance and consequent electrical conductivity can be directly extracted from the ratio of voltage and current according to Ohms Law.

The suspended Pt nanofilm sensor integrated with the probing electrodes is fabricated on a double layered film of silicon oxide/silicon by electron beam (e-beam) lithography, e-beam physical vapor deposition, and etching processes[33] (fabrication details are presented in Supporting Information). The dimensions of the nanofilm sensor are 40.3 nm in thickness, 412.0 nm in width, and 9.552 μm in length, respectively. The gap between the nanofilm and substrate is

about 6 μm. The studied Bi_2S_3 nanowire is fabricated by hydrothermal synthesis using $Bi(NO_3)_3$ and $Na_2S_2O_3$ as raw materials, carbamide ($CO(NH_2)_2$) as pH modifier and ethanediol ($C_2H_6O_2$) as solvent.[34] Fig. 2 schematically shows the process of handling an individual Bi_2S_3 nanowire and fixing on the suspended Pt nanofilm sensor by using a nanomanipulator whose tip diameter is in the submicron range, which requires precise pre-alignment, i.e., highly tuned location and coordination, and precise focusing of the e-beam.[32,35] The as-synthesized Bi_2S_3 nanowires are ultrasonically dispersed in ethanol solution and dropped on a microgrid for transmission electron microscopy (TEM) [Fig. 2(a)]. A single Bi_2S_3 nanowire of high quality is selected, marked and the corresponding nanostructures are investigated by SEM and TEM. The selected nanowire is picked up by a sharpened tungsten probe attached on a commercial nanomanipulator (kleindiek MM3A-EM) in SEM. During this process, the tungsten probe first attracts the Bi_2S_3 nanowire by using electrostatic force and then e-beam induced Pt deposition is made to enhance the adhesion [Fig. 2(a)]. Fig. 2(b) gives the schematic view and the corresponding SEM image of the picked Bi_2S_3 nanowire. As shown in Fig. 2(c), the picked nanowire is placed on the pre-fabricated suspended Pt nanofilm sensor and conducted by the nanomanipulator. Subsequently, e-beam induced Pt deposition is made around the contact point to enhance the bonding and thus reduce the thermal and electrical resistance. Then, the nanowire is stretched toward the opposite electrode (heat sink) and e-beam induced Pt deposition is also applied. After successful fixing of the tested Bi_2S_3 nanowire across the suspended nanofilm sensor and electrode, the nanomanipulator mechanically detaches from the nanowire while another nanomanipulator, labeled as B, presses the nanowire to avoid damage to the contact point and the tested segment of the nanowire [Fig. 2(d)]. The SEM image of the as-fabricated sample is shown in Fig. 1(c). The diameter of the Bi_2S_3 nanowire is 153.4 nm and the length of the suspended section is 3.0 μm.

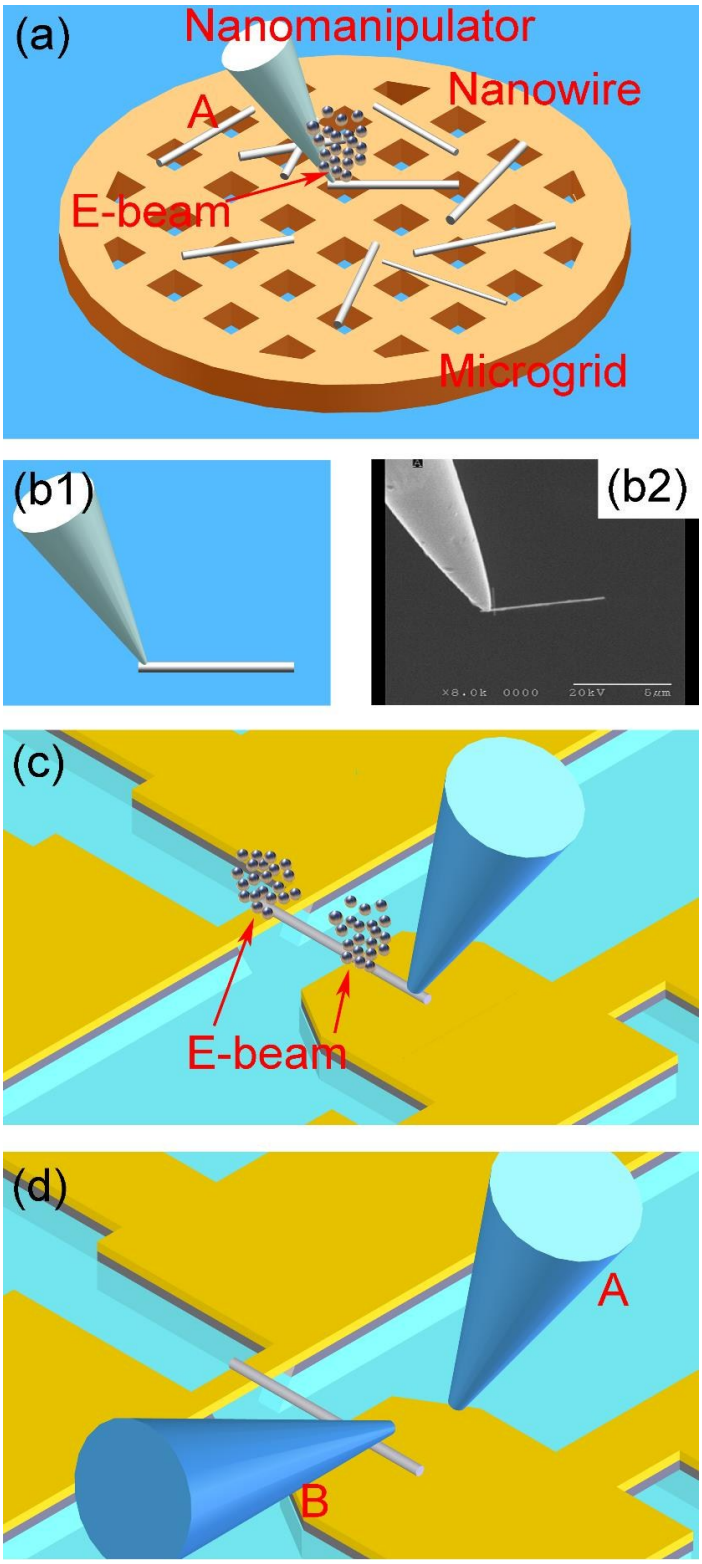

Fig. 2 Schematic diagram of picking up a single Bi_2S_3 nanowire and fixing on the suspended Pt nanofilm sensor.

In all measurements, the sample is mounted on the sample holder in a liquid nitrogen cryostat (Oxford Instruments, Optistat DN-V cryostat system). The sample chamber is continuously evacuated by a vacuum pump and a molecular pump so as to obtain and maintain a high vacuum level of 10^{-4} Pa. The temperature of the sample holder can be steadily controlled from 80 K to 500 K by the intelligent temperature controller (Oxford Instruments, ITC601PT) with an accuracy of ±0.1 K. The measurement system consists of the sample, a standard resistance, a high accuracy constant power supply (Advantest R6243), two high accuracy digital multimeters (Keithley 2002, 8.5digits), and a lock-in-amplifier (LIA, Stanford Research Systems, SR830). The constant power supply provides dc current for measuring the thermal and electrical conductivities of the Bi_2S_3 nanowire. The digital multimeters are used to detect the ohmic voltage in thermal and electrical conductivities measurement and dc thermoelectric voltage in the Seebeck coefficient measurement. The LIA serves to supply the ac current of the form $I_0\sin(\omega t)$ to heat the Pt nanofilm sensor as well as detect the ac ohmic voltage across the nanofilm in the sensor calibration and Seebeck coefficient measurement.

Results and discussion

The determined figure of merit of the Bi_2S_3 nanowire is illustrated in Fig. 3. It can be found that the *ZT* is far less than the reported values of nanostructured bulk Bi_2S_3 samples. The maximum value of *ZT* is 1.76×10^{-4} at 280 K and the minimum value is 1.28×10^{-6} at 300 K. Correspondingly, the reported maximum and minimum *ZT* are 0.12 at 420 K on nanonetwork hot-pressed bulk[29] and 2×10^{-9} at 373 K on single crystalline pellets.[22] To explore the mechanism responsible for the low figure of merit, the Seebeck coefficient, thermal and electrical conductivities have been studied respectively.

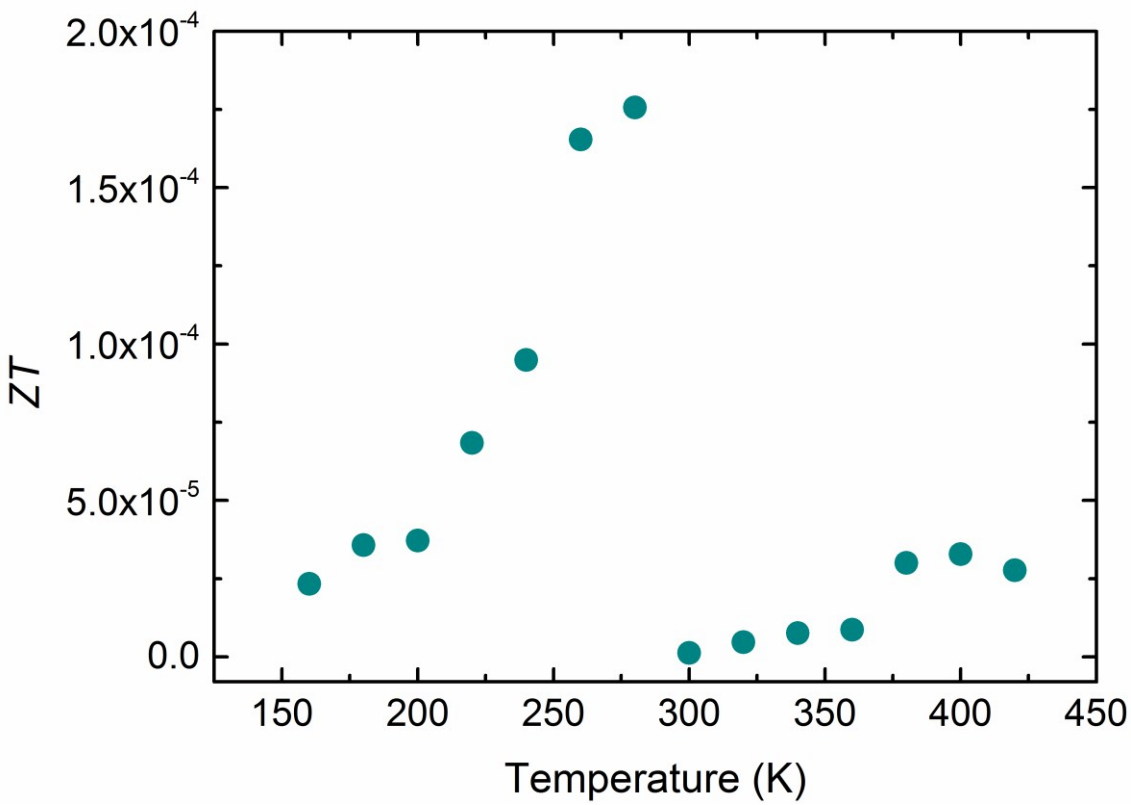

Fig. 3 Figure of merit of the individual single crystal Bi_2S_3 nanowire versus temperature.

The temperature dependent electrical resistivity and Seebeck coefficient are illustrated in Fig. 4. The room temperature electrical resistivity is 1.57 Ω cm, corresponding to the value of hydrothermal synthesized single Bi_2S_3 nanowire, 1.2 Ω cm.[36] The electrical resistivity versus temperature data exhibits a peak at 200 K. Below 200 K, the temperature dependence is positive, $d\rho/dT>0$, exhibits metallic characteristics, and above 200 K, the temperature dependence is negative, $d\rho/dT<0$. The inset shows a logarithmic plot of resistivity versus reciprocal temperature. The plot is almost linear above 240 K indicating that the resistivity exhibits a typical semiconductor Arrhenius behavior with activated-type conduction according to the relation,

$$\rho(T) = \rho_0 \exp\left(\frac{E_0}{k_B T}\right) \quad (6)$$

where k_B is Boltzmann's constant, E_0 is activation energy, and ρ_0 is pre-exponential factor. The determined activation energy E_0 is 0.297 eV. Bi_2S_3 is a semiconductor with a direct bandgap of 1.3 eV. The activation energy is about one quarter of the thermal band gap energy, indicating that above 240 K the electrical conduction is extrinsic and dominated by the concentration of the charge carriers generated by ionization of impurity levels. One possible mechanism responsible for the present metal-insulator transition is extrinsic-intrinsic transition with increasing temperature.[37-39] In the temperature range from 160 K to 200 K, all of the impurity donors are thermally activated and the intrinsic carriers are not yet excited to a marked degree. The carrier concentration remains approximately constant and equal to the impurity concentration. Therefore, the temperature dependence of resistivity is determined by that of the carrier mobility which falls due to the scattering by acoustical and optical phonons, and ionized impurities. Above 220 K, the number of carriers thermally excited across the semiconducting energy gap begins to be dominant.

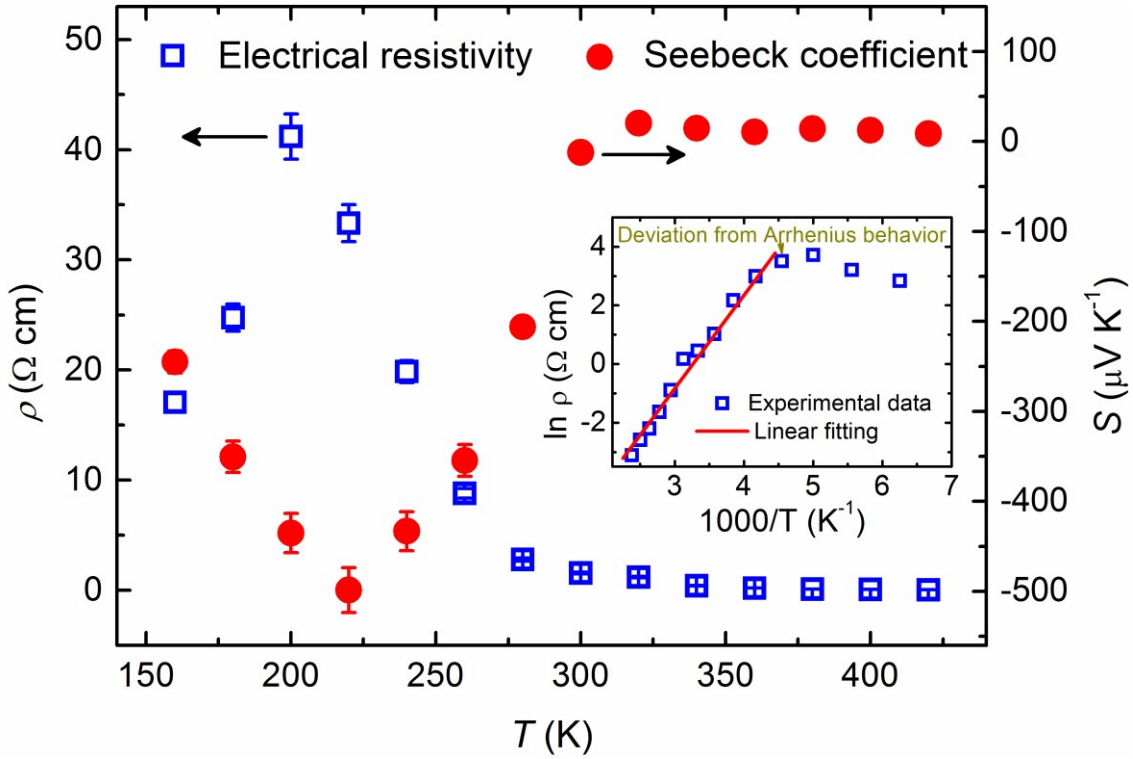

Fig. 4 Electrical resistivity and Seebeck coefficient of the individual single crystal Bi_2S_3 nanowire versus temperature.

The negative Seebeck coefficient at low temperature, from 160 K to 300 K, suggests that the transport characteristic is n-type and the electrons are the dominant carriers. The transition of the Seebeck coefficient from "-" to "+" at 320 K, which is the first observation on Bi_2S_3 samples, indicates that the mobility of the holes becomes higher than that of the electrons. The Seebeck coefficient transition at temperature as low as 320 K also reflect the good quality of the Bi_2S_3 nanowire, since deviations from stoichiometry would increase the electron concentration at the expense of the hole concentration.[40] The Seebeck coefficient is nearly zero in the temperature range of 300 - 420 K, mainly responsible for the ultralow figure of merit. The Seebeck coefficient exhibits a dip at 220 K, corresponding roughly to the maximum in resistivity except little difference which is attributed to the limited measurement interval. As stated in the electrical

resistivity analysis, in the extrinsic region from 160 K to 200 K, the carrier mobility is dominant and tends to decrease due to the scattering, and consequently decreases the absolute value of Seebeck coefficient. In the intrinsic region above 220 K, the number of carriers thermally excited across the impurity level ionization energy begins to be dominant, which results to the decrease of the Seebeck coefficient.

Fig. 5 compares the temperature dependent thermal conductivities of the present nanowire and other reported Bi_2S_3 samples, i.e., ingots,[24,41] SPS-sintered polycrystalline bulk,[25,27] nanonetwork hot-pressed bulk,[29] bulk single crystals,[42] and single crystalline pellets.[43] The thermal conductivity of the present Bi_2S_3 nanowire lies in the range of 2.2-2.6 W m^{-1} K^{-1} with insignificant temperature dependence, which is similar to that of $Bi_{1-x}Te_x$ nanowire,[44] Bi_2Te_3 nanowire,[45] $CrSi_2$ nanowire,[46] InSb nanowire,[47] and ZnTe nanowire.[48] The electronic thermal conductivity estimated based on the Wiedemann-Franz law is much smaller than the measured thermal conductivity, indicating that phonons dominate heat conduction in Bi_2S_3 nanowire. In the present temperature range, the thermal conductivity reaches a plateau at about 180 K and subsequently starts to decrease with increasing temperature which indicates Umklapp scattering is still the dominant phonon scattering process. At high temperature, the thermal conductivity increases gradually with temperature, which can be attributed to the onset of bi-polar diffusion at higher temperature. It can be found that the thermal conductivity of the present nanowire is larger than most of the reported values, compared to that of the single crystals, and smaller than the value, 42.2 W m^{-1} K^{-1} of the single crystalline pellets. Generally, the thermal conductivity of nanowire significantly decreases compared to the corresponding bulk value, i.e., Si nanowire,[11,49] due to the phonon-boundary scattering. To explore the mechanism responsible for this opposite trend, the structure of the Bi_2S_3 nanowire was studied.

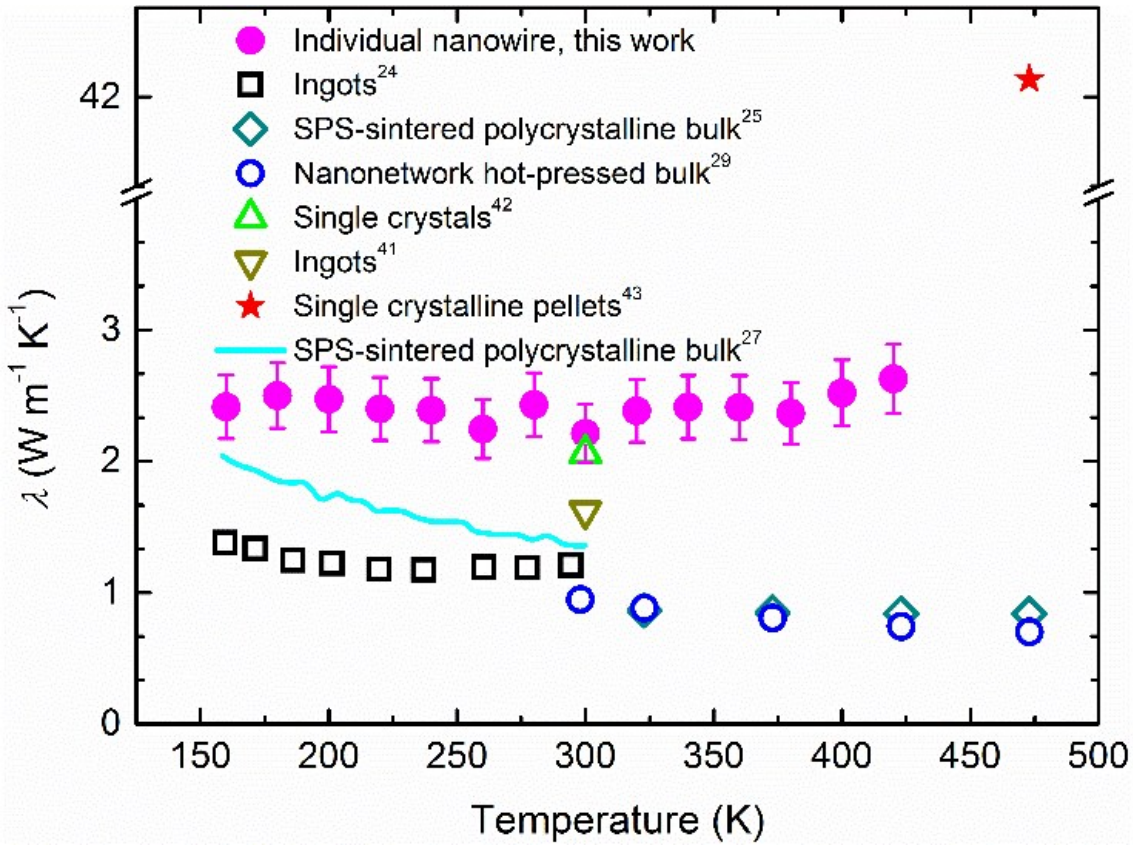

Fig. 5 Comparison of the temperature dependent thermal conductivity for different Bi_2S_3 samples.

The high-resolution transmission electron microscopy (HRTEM) image and the corresponding selected area electron diffraction (SAED) are shown in Fig. 6. The observed lattice spacings of 0.57 nm and 0.40 nm correspond to the (020) and (001) planes of the orthorhombic B_2S_3 (PDF#17-0320). The SAED pattern reveals that the nanowire is single crystal. Both the HRTEM image and SAED pattern indicate that the growth direction of the highly crystalline Bi_2S_3 nanowire is consistent with the crystallographic *c*-axis. In this direction, the layered crystal structure consists of $[Bi_2S_3]_\infty$ chains. The $[[Bi_2S_3]_2]_\infty$ ribbons formed by pairs of $[Bi_2S_3]_\infty$ chains are connected to form layers. The distinctive features of the layered crystals are quasi-one-dimensional with non-equivalent positions of atoms and the corresponding complicated (covalent, ionic-covalent, metallic, and donor-acceptor) chemical bondings. The

quasi-one-dimensional crystals form parallel channels for heat conduction. That is the mechanism responsible for the larger thermal conductivity of single crystalline Bi_2S_3 samples compared to nanostructured polycrystalline bulks, especially in the *c*-axis. It is expected that the nanowire boundary scattering will hinder the thermal transport. However, the thermal conductivity of the present *c*-axis oriented highly crystalline Bi_2S_3 nanowire is still larger. Conversely, the thermal conductivity of the nanostructured polycrystalline bulks is expected to decrease significantly.

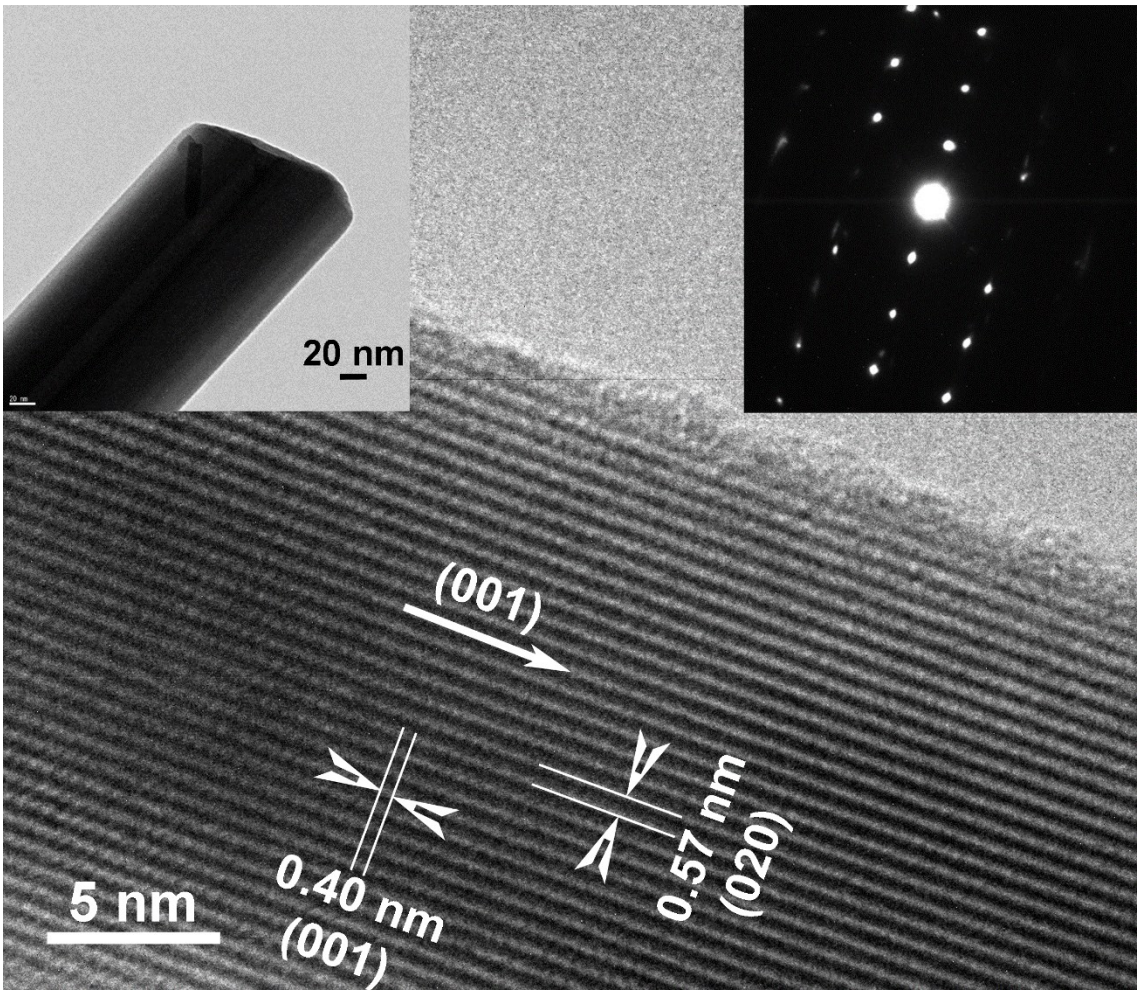

Fig. 6 High-resolution TEM image of the Bi_2S_3 nanowire, the inset showing the corresponding TEM and SAED pattern.

Conclusions

A T-type method to comprehensively characterize the thermoelectric performance of one-dimensional nanostructures has been first developed. The thermoelectric performance including Seebeck coefficient, thermal conductivity and electrical conductivity of an individual free-standing single crystal Bi_2S_3 nanowire in the temperature range from 160 K to 420 K have been first determined by applying the T type method with the help of focused electron beam-assisted nanomanipulation. The maximum value of *ZT* is 1.76×10^{-4} at 280 K, which is far less than the reported values of nanostructured bulk Bi_2S_3 samples. The resistivity versus temperature data shows a peak at 200 K and exhibits an Arrhenius-type behavior above 240 K. The Seebeck coefficient is nearly zero in the temperature range of 300-420 K and changes its sign at 320 K. The thermal conductivity is larger than the reported value of nanostructured polycrystalline Bi_2S_3 bulks.

Acknowledgements

This work was supported by the National Natural Science Foundation of China (Grant Nos. 51406236, 51206094, 51576105, 51327001, and 51336009), High-Tech 973 Program of China (Grant No. 2013CB632503), Science Foundation of China University of Petroleum, Beijing (2462013YJRC027), and Science Fund for Creative Research Groups (No. 51321002), and China Postdoctoral Science Foundation.

References

1 L. D. Zhao, S. H. Lo, Y. Zhang, H. Sun, G. Tan, C. Uher, C. Wolverton, V. P. Dravid and M. G. Kanatzidis, *Nature*, 2014, **508**, 373.

2 S. W. Lee, Y. Yang, H. W. Lee, H. Ghasemi, D. Kraemer, G. Chen and Y. Cui, *Nat. Commun.*, 2014, **5**, 3942.

3 J. F. Li, W. S. Liu, L. D. Zhao and M. Zhou, *NPG Asia Mater.*, 2010, **2**, 152.

4 H. Bottner, G. Chen and R. Venkatasubramanian, *MRS Bull.*, 2006, **31**, 211.

5 A. I. Hochbaum, R. Chen, R. D. Delgado, W. Liang, E. C. Garnett, M. Najarian, A. Majumdar and P. Yang, *Nature*, 2008, **451**, 163.

6 R. Venkatasubramanian, E. Siivola, T. Colpitts and B. O'Quinn, *Nature*, 2001, **413**, 597.

7 B. Poudel, Q. Hao, Y. Ma, Y. Lan, A. Minnich, B. Yu, X. Yan, D. Wang, A. Muto, D. Vashaee, X. Chen, J. Liu, M. S. Dresselhaus, G. Chen and Z. Ren, *Science*, 2008, **320**, 634.

8 T. C. Harman, P. J. Taylor, M. P. Walsh and B. E. LaForge, *Science*, 2002, **297**, 2229.

9 A. Shakouri and M. Zebarjadi, Nanoengineered Materials for Thermoelectric Energy Conversion. *In Thermal Nanosystems and Nanomaterials*, 2009, **118**, 225.

10 M. Zebarjadi, K. Esfarjani, M. S. Dresselhaus, Z. F. Ren and G. Chen, *Energy Environ. Sci.*, 2012, **5**, 5147.

11 D. Y. Li, Y. Y. Wu, P. Kim, L. Shi, P. D. Yang and A. Majumdar, *Appl. Phys. Lett.*, 2003, **83**, 2934.

12 L. Shi, D. Y. Li, C. H. Yu, W. Y. Jang, D. Kim, Z. Yao, P. Kim and A. Majumdar, *J. Heat Transfer*, 2003, **125**, 881.

13 R. Chen, A. I. Hochbaum, P. Murphy, J. Moore, P. Yang and A. Majumdar, *Phys. Rev. Lett.*, 2008, **101**, 105501.

14 J. W. Roh, K. Hippalgaonkar, J. H. Ham, R. Chen, M. Z. Li, P. Ercius, A. Majumdar, W. Kim and W. Lee, *ACS Nano*, 2011, **5**, 3954.

15 M. C. Wingert, Z. C. Y. Chen, E. Dechaumphai, J. Moon, J. H. Kim, J. Xiang and R. Chen, *Nano Lett.*, 2011, **11**, 5507.

16 J. Grigas, E. Talik and V. Lazauskas, *Phys. Stat. Sol. B*, 2002, **232**, 220.

17 X. Tang, W. Xie, H. Li, W. Zhao, Q. Zhang and M. Niino, *Appl. Phys. Lett.*, 2007, **90**, 012102.

18 R. Chmielowski, D. Pere, C. Bera, I. Opahle, W. Xie, S. Jacob, F. Capet, P. Roussel, A. Weidenkaff, G. K. H. Madsen and G. Dennler, *J. Appl. Phys.*, 2015, **117**, 125103.

19 X. Du, F. Cai and X. Wang, *J. Alloys Compd.*, 2014, **587**, 6.

20 K. Biswas, L. D. Zhao and M. G. Kanatzidis, *Adv. Energy Mater.*, 2012, **2,** 634.

21 H. T. Shaban, M. M. Nassary and M. S. El-Sadek, *Physica B*, 2008, **403**, 1655.

22 A. B. K. Chen, S. G. Kim, Y. Wang, W. S. Tung and I. W. Chen, *Nat. Nano.*, 2011, **6**, 237.

23 H. Mizoguchi, H. Hosono, N. Ueda and H. Kawazoe, *J. Appl. Phys.*, 1995, **78**, 1376.

24 B. X. Chen, C. Uher, L. Iordanidis and M. G. Kanatzidis, *Chem. Mater.*, 1997, **9**, 1655.

25 L. D. Zhao, B. P. Zhang, W. S. Liu, H. L. Zhang and J. F. Li, *J. Solid State Chem.*, 2008, **181**, 3278.

26 Z. H. Ge, B. P. Zhang, P. P. Shang, Y. Q. Yu, C. Chen and J. F. Li, *J. Electron. Mater.*, 2011, **40**, 1087.

27 Y. Kawamoto and H. Iwasaki, *J. Electron. Mater.*, 2014, **43**, 1475.

28 Z. H. Ge, B. P. Zhang, P. P. Shang and J. F. Li, *J. Mater. Chem.*, 2011, **21**, 9194.

29 W. Liu, C. F. Guo, M. Yao, Y. Lan, H. Zhang, Q. Zhang, S. Chen, C. P. Opeil and Z. Ren, *Nano Energy*, 2014, **4**, 113.

30 Q. Yang, C. Hu, S. Wang, Y. Xi and K. Zhang, *J. Phys. Chem. C*, 2013, **117**, 5515.

31 S. C. Liufu, L. D. Chen, Q. Yao and C. F. Wang, *Appl. Phys. Lett.*, 2007, **90**, 112106.

32 M. Fujii, X. Zhang, H. Q. Xie, H. Ago, K. Takahashi, T. Ikuta, H. Abe and T. Shimizu, *Phys. Rev. Lett.*, 2005, **95**, 065502.

33 Q. G. Zhang, B. Y. Cao, X. Zhang, M. Fujii and K. Takahashi, *J. Phys.: Condens. Matter*, 2006, **18**, 7937.

34 Z. H. Ge, B. P. Zhang, Z. X. Yu and B. B. Jiang, *CrystEngComm*, 2012, **14**, 2283.

35 J. Hirotani, T. Ikuta, T. Nishiyama and K. Takahashi, *Nanotechnology*, 2011, **22**, 315702.

36 Y. Yu, C. H. Jin, R. H. Wang, Q. Chen and L. M. Peng, *J. Phys. Chem. B*, 2005, **109**, 18772.

37 E. M. Conwell, *Proc. IRE*, 1952, **40**, 1327.

38 J. Hu, T. F. Rosenbaum, *Nature Mater.*, 2008, **7**, 697.

39 V. L. Kuznetsov, L. A. Kuznetsova, D. M. Rowe, *J. Appl. Phys.*, 1999, **85**, 3207.

40 J. M. Lopezcastillo, A. Amara, S. Jandl, J. P. Jaygerin, C. Ayache and M. J. Aubin, *Phys. Rev. B*, 1987, **36**, 4249.

41 A. C. Glatz and V. F. Meikleham, *J. Electrochem. Soc.*, 1963, **110**, 1231.

42 L. Gildart, J. M. Kline and D. M. Mattox, *J. Phys. Chem. Solids*, 1961, **18**, 286.

43 M. P. Deshpande, P. N. Sakariya, S. V. Bhatt, N. H. Patel, K. Patel and S. H. Chaki, *Bull. Mater. Sci.*, 2015, **38**, 83.

44 A. Mavrokefalos, A. L. Moore, M. T. Pettes, L. Shi, W. Wang and X. Li, *J. Appl. Phys.*, 2009, **105**, 104318.

45 C.-L. Hsin, M. Wingert, C.-W. Huang, H. Guo, T.-J. Shih, J. Suh, K. Wang, J. Wu, W.-W. Wu and R. Chen, *Nanoscale*, 2013, **5**, 4669.

46 F. Zhou, J. Szczech, M. T. Pettes, A. L. Moore, S. Jin and L. Shi, *Nano Lett.*, 2007, **7**, 1649.

47 F. Zhou, A. L. Moore, M. T. Pettes, Y. Lee, J. H. Seol, Q. L. Ye, L. Rabenberg and L. Shi, *J. Phys. D: Appl. Phys.*, 2010, **43**, 025406.

48 K. Davami, A. Weathers, N. Kheirabi, B. Mortazavi, M. T. Pettes, L. Shi, J.-S. Lee and M. Meyyappan, *J. Appl. Phys*., 2013, **114**, 134314.

49 A. I. Boukai, Y. Bunimovich, J. Tahir-Kheli, J.-K. Yu, W. A., III Goddard and J. R. Heath, *Nature*, 2008, **451**, 168.

Table of contents

Comprehensive T-type method is developed to evaluate the thermoelectric performance of one-dimensional nanostructures and individual Bi_2S_3 nanowire is studied.

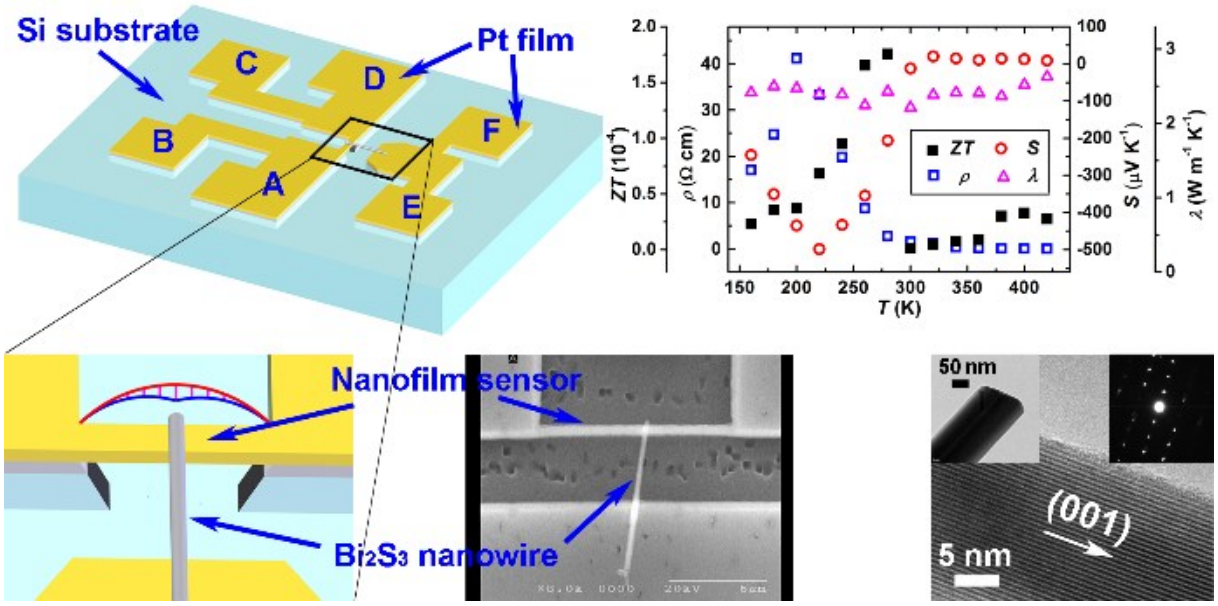

TOC graphic (Zhang)